Power Electronic Systems
Laboratory

Proceedings of the 9th International Conference on Power Electronics (ECCE Asia 2015), Seoul, South Korea, June 1-5, 2015

Advanced Cooling Concepts for Ultra-High-Speed Machines

A. Tüysüz,
M. Steichen,
C. Zwyssig,
J. W. Kolar

Eidgenössische Technische Hochschule Zürich
Swiss Federal Institute of Technology Zurich

Advanced Cooling Concepts for Ultra-High-Speed Machines

A. Tüysüz[1], M. Steichen[1], C. Zwyssig[2] and Johann W. Kolar[1]
[1] Power Electronic Systems Laboratory, ETH Zurich, Switzerland
[2] Celeroton AG, Switzerland

***Abstract*-- High-speed electrical machines are gaining an increasing attention as they enable higher power densities in several applications such as micro-machining spindles and turbo compressors. This brings along an important challenge in thermal management due to the higher loss densities in the machine. Therefore, a careful thermal analysis is required along with the electromagnetic and mechanical analysis during the design phase of the machines. In this paper, five different forced cooling options for a slotless-type ultra-high-speed permanent-magnet machine are compared. Fast and sufficiently accurate thermal models are derived for analyzing these cooling concepts such that the cooling system design could be integrated in the machine optimization procedure, which would not be feasible when using computationally very intensive methods such as 3-D Finite-Element-Method (FEM) or Computational-Fluid-Dynamics (CFD).**

Measurements are carried out on the stator of an off-the-shelf 1 kW, 280 000 r/min machine to experimentally compare different cooling methods and to show the validity of the thermal models. A simplified case study shows that the power density can be more than doubled by the selection of a proper cooling system.

***Index Terms* — High-speed drives, modeling, cooling.**

I. Introduction

High-speed electrical drives have been a very popular research topic lately. In the last decade, both academia and industry have been working intensively on high-speed machine concepts due to the higher power density and improved reliability that high-speed drive systems offer [1]. Especially in the last decade, ultra-high-speed drive systems have found new application areas in portable power generation, turbo compressors and spindles [2], [3]. Furthermore, a major part of the research in electrical machinery is expected to be about high-speed drives in the near future due to both the advancements in enabling technologies (e.g., magnetic and gas bearings, higher-quality core materials, self-sensing techniques for low-saliency machines etc.) and the advantages that high-speed drives bring in several applications [1].

For a given power rating and cooling capability, increasing the rotational speed of an electrical machine results in lower machine volume and weight, hence higher power density [4]. This is especially beneficial in mobile applications such as heating, ventilation and air conditioning as well as turbocharging of higher-efficiency, more-electric drivetrain of automobiles and electric cabin pressurization compressors of airplanes [1], [5]. As examples, a 500 000 r/min, 150 W electrically driven turbo compressor is presented in [5], and the design methodology for a 500 000 r/min, 100 W electrical machine is given in [6]. Similarly, reaction wheels used for attitude control of small satellites benefit from a reduced weight and increased angular momentum density with higher rotational speeds. For instance, a 250 000 r/min motor with a novel active magnetic bearing topology is investigated for small satellite reaction wheels in [7]. Finally, an ultra-high-speed electric motor running at 1 000 000 r/min is presented as the world's fastest electrical drive in [8].

In ultra-high-speed drives, besides increased mechanical stresses in the rotor and rotor dynamics constraints, thermal considerations become more important due to the higher loss densities resulting from a smaller volume and surface area. In order to design a reliable and optimum machine, the traditional way of optimization considering only electromagnetic and mechanical aspects for a given specific electric loading cannot be taken anymore, and the thermal design needs to be part of the machine design and optimization procedure [9]. Combined thermal and electromagnetic analyses of electric machines are carried out in [10] by using a commercial software and in [11] by presenting a model for the electromagnetic-thermal problem in a weakly coupled form.

The slotless permanent-magnet (PM) machine topology (Fig. 1) is usually preferred for high-speed drives (above 200 000 r/min), due to the weaker armature fields and thus lower rotor losses. Furthermore, the slotless configuration means that stator core saturation or demagnetization of the rotor permanent magnet is

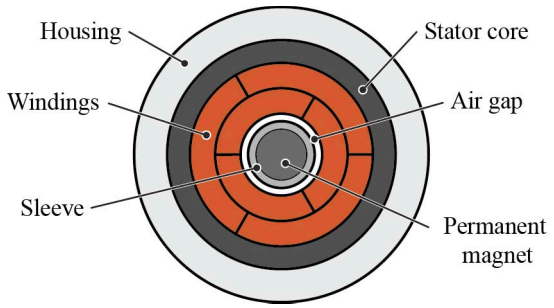

Fig. 1. Conceptual representation of the cross-sectional area of a slotless PM machine with skewed-type air gap windings. The windings are depicted symmetrically (one inner and one outer layer coil side per phase); however, in practice it may look differently depending on the axial location of the cross-sectional view.

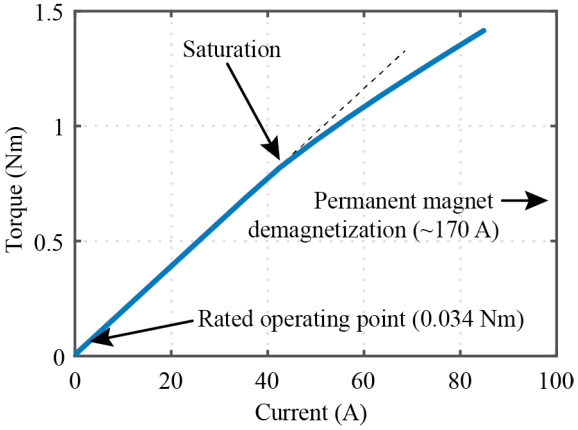

Fig. 2. Dependency of the torque of the 2-pole slotless PM machine (Table I) on the phase current. Saturation of the stator core starts appearing in the torque-current curve only at around twenty times the rated current. An even higher current is required to demagnetize the rotor magnet[i].

possible only by having unpractically high current densities in the windings. As an example, Fig. 2 shows the relationship between the torque and the phase current for an off-the-shelf 1 kW, 280 000 r/min slotless PM machine [12] that is being used as a case study in this work. It is clearly seen that the electromagnetic limits are not close to the rated operating point of the machine. Therefore, it can be concluded that the rated torque of these machines is almost always set by the thermal limits. Consequently, the torque density and hence the power density of the machine can be increased by using a higher-performance cooling system.

This paper describes several different forced cooling concepts for a slotless-type high-speed PM machine. Both air and water are considered as coolants as they are easily available in various applications. Fast and sufficiently accurate thermal models are derived for describing these forced cooling methods such that the cooling system analysis could be made part of the machine optimization procedure, which is not the case with the computationally very intensive methods such as 3-D Finite-Element-Method (FEM) or Computational-Fluid-Dynamics (CFD).

In order to show the validity of the thermal models, different stators are manufactured by integrating the analyzed forced cooling methods into an off-the-shelf 280 000 r/min, 1 kW electric machine by keeping the original magnetic design. A simplified case study shows that the torque and hence the power density can be more than doubled by the selection of a proper cooling system.

II. Thermal Modeling of Forced Cooling Concepts for Slotless PM Machines

A. Thermal Modeling of the Slotless PM Machine

A conceptual representation of the slotless PM machine topology is shown in Fig. 1. The stator core is made of a hollow-cylinder shaped stack of laminated amorphous iron (sheet thickness ~ 20 µm). Air gap windings are used and these two components are bound using epoxy casting. Skewed-type air gap windings made of litz wire are used in order to limit the axial space required for the end windings. The rotor consists of a diametrically magnetized cylindrical magnet, and a retaining sleeve made of titanium. The sleeve ensures mechanical stability and also transfers the torque to the load of the machine. This machine concept is used for implementing the electric motor of the commercially available turbo compressor CT-17-1000 from Celeroton AG [12], which is considered in this work as a case study. Table I summarizes key parameters of this machine.

TABLE I
Key Parameters of the Machine Considered in This Work

Rated speed	280 000 r/min
Rated power	1 kW
Pole pair number	1
PM flux linkage	6 10^{-3} Vs
Rated efficiency	0.94
Rotor axial moment of inertia	5.5 10^{-7} kgm^2
Phase resistance	0.85 Ω
Phase inductance	130 µH
Rotor diameter	11 mm
Axial length	33 mm
Winding bore diameter	12.5 mm
Stator outer diameter	27.5 mm

As described in detail in [14], methods for thermal analysis of electrical machines can be grouped into lumped-parameter networks, FEM and CFD. Even though complicated geometries can be modeled using the latter two, they are computationally very intensive and cannot be used at the machine optimization phase easily.

Therefore, in this work, a lumped-parameter-based method is adopted for thermal analysis. Firstly, the geometry of the machine is discretized in 3-D[ii] as shown in Fig. 3. This results in the representation of the machine geometry by a set of small arc-shaped elements as shown in Fig. 4 (a), for which the conductive thermal resistances in radial ($R_{\mathrm{th,ra}}$), axial ($R_{\mathrm{th,ax}}$) and azimuthal[iii] ($R_{\mathrm{th,az}}$) directions can be calculated as

$$R_{\mathrm{th,ra}} = \frac{\ln(r_\mathrm{o}/r_\mathrm{i})}{\lambda_{\mathrm{ra}}\varphi l} \quad (1)$$

$$R_{\mathrm{th,ax}} = \frac{2l}{\lambda_{\mathrm{ax}}\varphi(r_\mathrm{o}^2-r_\mathrm{i}^2)} \quad (2)$$

$$R_{\mathrm{th,az}} = \frac{\varphi(r_\mathrm{o}^2-r_\mathrm{i}^2)}{2\lambda_{\mathrm{az}} l(r_\mathrm{o}-r_\mathrm{i})^2} \quad (3)$$

where r_o, r_i, l and φ define the arc shape (Fig. 4 (a)). λ_{ra}, λ_{ax}, λ_{az} are the specific thermal conductivities of the material in the radial, axial and azimuthal directions.

[i] The inclination of the demagnetizing field is neglected and all field is assumed to be antiparallel to the direction of the magnetic polarization of the permanent magnet. The field inclination needs to be taken into account for a more accurate demagnetization calculation [13].

[ii] Some of the cooling concepts described later have changing geometries in the azimuthal direction and thus require a 3-D modeling, whereas some others are symmetric around the azimuthal axis and can be modeled using an axisymmetric 2-D model. For generality, all the models are developed in 3-D. Only one element can be used in the azimuthal direction for modeling the axisymmetric cases.

[iii] The azimuthal heat path depends on the radius where it is evaluated. Here, the mean thermal resistance is considered.

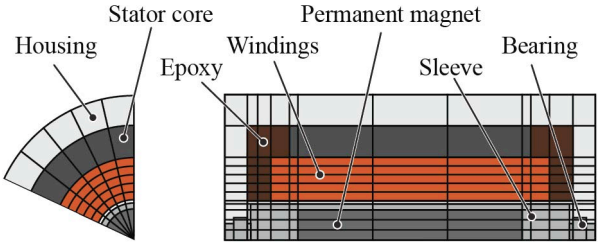

Fig. 3. Discretization of the machine geometry for thermal analysis.

The thermal behavior of the machine is analyzed by constructing a thermal network where each arc-shaped element is represented by six thermal resistances in the three axes connected to a center node as shown in Fig. 4 (b). For solid domains (where heat is transferred by conduction), each arc-shaped element is further divided into two halves in all three axes and the equations (1)-(3) are used to calculate the values of the six thermal resistances shown in Fig. 4 (b). Anisotropic thermal conductivities of the laminated stator core or the winding pack can easily be accounted for assuming different thermal conductivity values in different axes.

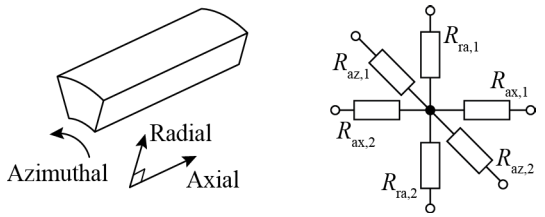

Fig. 4. (Left) Basic arc-shaped thermal element. (Right) Representation of the arc-shaped element with six thermal resistors in radial, axial and azimuthal directions.

In this representation, the center node coincides with the geometric center of the arc-shaped element, which is assumed to be of uniform temperature. The losses associated with that element (e.g. copper losses, if the element is representing part of the windings) are introduced at the center node considering the loss density in the machine and the volume of that specific element.

Following the treatment of the thermal resistances representing the conductive heat transfer and the heat sources representing the losses, the convective heat transfer that takes place in the air gap and in the forced air/water cooling channels needs to be treated in a similar fashion.

The thermal conductivity of the air gap is calculated according to [15], taking the air gap geometry and the rotational speed of the rotor into account.

In this work, the commonly used jacket cooling is compared to four more advanced forced cooling methods in which the coolant flows in channels having the form of either round-shaped ducts or annular gaps, both in the axial direction of the machine. Empirical formulae describing the heat transfer into the coolant flowing in these channels are given in [16]. The Nusselt number (Nu) can be obtained using these formula based on whether the flow is laminar, mixed or turbulent. The equivalent thermal resistance $R_{\mathrm{th,fl}}$ can be calculated based on the heat transfer coefficient h as

$$h = \frac{Nu\,\lambda}{d_{\mathrm{h}}} \tag{4}$$

$$R_{\mathrm{th,fl}} = \frac{1}{hA_{\mathrm{we}}} \tag{5}$$

where d_{h} is the hydraulic diameter of the channel, A_{we} is the wetted surface and λ is the thermal conductivity of the coolant [16].

Even though the analysis is carried out on simplified geometries as explained above, the convective heat transfer is more complicated to analyze compared to its conductive counterpart, due to the need of iterative computation. Firstly, the thermal resistance is calculated based on the wall surface and the fluid temperatures as well as the fluid's physical properties. With this, the heat transfer to/from the fluid is calculated, resulting in a change in the fluid temperature. This is repeated with the updated fluid temperature until the results converge.

Once the geometric discretization is carried out, the thermal resistance network set up and the losses introduced as described above, the steady-state temperature of each element is found by solving the system as described in detail in [17].

The laminated structure of the stator core results in a highly anisotropic thermal conductivity. A strong anisotropy is also observed in the thermal conductivity inside the winding pack (litz wire - epoxy composite). An analytic calculation of the thermal resistances in different directions are possible for the windings [18], but it relies on the exact information of the geometric distribution of individual strands in the winding pack, which is challenging to obtain for skewed-type air gap windings. As the coolant is applied over the whole axial length of the machine for all the forced cooling methods considered in this work, the main heat flow is in the radial and azimuthal directions into the cooling channels. Therefore, the radial and azimuthal thermal conductivities of the winding pack are of higher importance. The specific radial thermal conductivity is measured on an existing winding pack with similar structure but different dimensions, and used for calculating the thermal resistance in the radial direction. The azimuthal thermal conductivity is assumed to be the same as the radial. The axial thermal conductivity ($\lambda_{\mathrm{wi,ax}}$) of the winding pack is approximated by

$$\lambda_{\mathrm{wi,ax}} = c_{\mathrm{sk}}(\lambda_{\mathrm{cu}}k_{\mathrm{cu}} + \lambda_{\mathrm{in}}k_{\mathrm{in}} + \lambda_{\mathrm{ep}}k_{\mathrm{ep}}) \tag{6}$$

where the λ_{cu}, λ_{in}, λ_{ep} are the thermal conductivities and the k_{cu}, k_{in}, k_{ep} are filling factors [iv] of the copper, insulation material (covering the copper strands) and the epoxy in the winding pack, respectively. The empirical constant $c_{\mathrm{sk}} \approx 0.1$ is introduced in order to take the skew of the windings and the twist of the bundles in the litz wire into account. Table II summarizes the thermal conductivities for the winding pack and the stator core.

[iv] Filling factor of a component is defined as the ratio of its total volume to the total winding pack volume.

A 60-µm thick polyimide tape is modeled at the winding pack – stator core interface. Even though it can easily be incorporated in the model, the thermal conductivity of the bearings are neglected at this step for simplicity. Natural convection and radiation from the outer surface of the housing are also neglected.

TABLE II
THERMAL CONDUCTIVITIES OF WINDING PACK AND THE STATOR CORE IN W/(MK)

Winding pack	Radial	1.8
	Axial	11
	Azimuthal	1.8
Stator core	Radial	9
	Axial	5
	Azimuthal	9

B. Forced Cooling Methods

1) Jacket Cooling

Jacket cooling is the current cooling method employed in the off-the-shelf electrical machine that is used in this work as a case study. In this method, the coolant (air or water) flows outside the machine housing shown in Fig. 1. The electromagnetic design of the machine is decoupled from the cooling system design, i.e., a cooling jacket can be built around any machine that has been optimized considering only electromagnetic and mechanical aspects. However, this results in a suboptimal cooling performance, as the thermal interface between the coolant and the critical parts of the machine (windings and permanent magnet) shows a relatively high resistance.

The collection of empirical formulae describing the convective heat transfer into coolants flowing in widely used channel shapes (as summarized in [16]) cannot be applied to the jacket cooling method considered in this work due to the significantly different channel geometry. However, assuming the coolant flow rate and the machine efficiency are sufficiently high, jacket cooling can be modeled in the first step as a fixed temperature (temperature of the coolant) on the outermost boundary of the housing (Fig. 3). The discretization of the geometry is carried out considering the trade-off between the computational effort and an adequate representation of the machine's thermal behavior; the geometry is discretized using 13 radial and 11 axial elements.

2) Heat Pipes Made of Graphite Sheets

If the time-harmonic content of the stator currents resulting from inverter switching is neglected, copper losses depend quadratically on the torque of the machine. Therefore, the thermal connection between the winding region and the coolant needs to be improved for increasing the power output of the machine.

Today, graphite sheets with thicknesses around 100 µm and thermal conductivities around 700 W/(mK) are commercially available. In this work, these sheets are utilized as heat pipes placed in the winding pack, thermally connecting the windings to the machine housing. An annular gap, in which the coolant flows, is introduced in the machine housing to remove the heat.

Fig. 5 depicts the modified thermal model that is used to analyze the use of the graphite heat pipes in the winding region. Even though the through-plane thermal conductivities of the graphite sheets is significantly lower than their in-plane thermal conductivities, the sheets are assumed to be isotropic and modeled with one segment in the radial direction per sheet, owing to the fact that they are very thin and the temperature distribution in the radial direction can be assumed to be uniform.

The ideal placement of the graphite sheets would be in the winding pack as shown in Fig. 5. However, for easier manufacturing they are placed only at the inner and outer surfaces of the winding pack. Moreover, the graphite sheets are covered by a 60 µm thick polyimide tape for mechanical stability at the expense of decreased overall thermal conductivity. A total of 16 4 mm wide graphite sheets are used, 8 placed on the outer and 8 on the inner surface of the windings, equally spaced (45° apart) in the azimuthal direction. The rotational symmetry is utilized and the geometry is represented with 16 radial, 14 axial and 5 azimuthal elements.

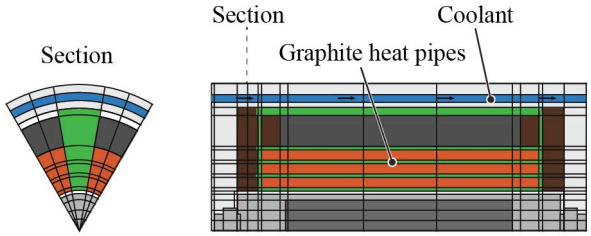

Fig. 5. Discretization of the machine geometry for the modified thermal model that is used to analyze the use of the graphite heat pipes in the winding region.

The graphite sheets have an electrical conductivity of 10 000 S/cm; accordingly the air gap field results in eddy-current losses in the sheets, which are calculated according to [19] and found to be in the milliwatt range for a 4 mm wide, 30 mm long and 0.1 mm thick graphite sheet placed in the case study machine when the machine is rotating at 280 000 r/min.

3) Toroidal Windings

Toroidal windings with slotless stator cores (Fig. 6) have been proposed as an alternative winding topology for different applications [20], [21], [22]. Compared to the skewed-type windings that are more widely used in high-speed slotless machines, the toroidal winding has the disadvantage that more than half of the total length is not used for torque production, but contributes to the copper losses. On the other hand, as windings are parallel to the axis of rotation, the winding factor is higher compared to the skewed windings. Moreover, the copper itself can be used as a thermally low-resistive path to the machine housing when toroidal windings are used.

Fig. 7 shows the thermal model used to analyze machine with toroidal windings. A finer discretization is applied to the winding geometry in order to resolve the corners where the copper is bent. The cross-sectional areas of the stator core and the windings inside the core are kept constant, which leads to an increased overall

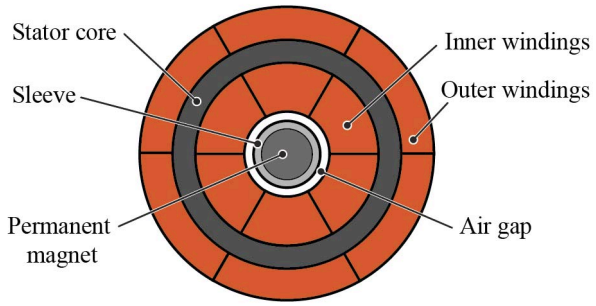

Fig. 6. Conceptual drawing of the cross-sectional area of a slotless PM machine with toroidal windings.

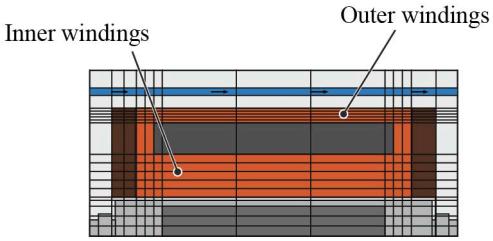

Fig. 7. Discretization of the machine geometry for the thermal analysis of the machine with toroidal windings.

machine volume due to the additional winding region outside the stator core. The geometry is modeled with 19 radial and 12 axial elements.

4) Axial Ducts

In the methods described above, the coolant flow has been kept outside the electromagnetically active part of the machine, and thermally low-resistive paths to the coolant have been investigated to conduct the heat generated in the machine to outer surfaces. Another approach to cool the winding region is to bring the coolant flow closer to the windings. One way of doing this is by introducing axial ducts in the winding region. This clearly increases the overall thermal conductivity towards the coolant and decreases the temperature of the hot spots, but it also increases the copper losses as the total winding cross-sectional area is reduced. Therefore, the number and size of the axial ducts need to be optimized considering the trade-off between the heat transfer rate and copper losses. In this work 12 axial ducts are considered, each with a 1 mm^2 cross-sectional area.

Fig. 8 shows the model used to study the thermal behavior of the machine with axial ducts. In the azimuthal direction, the machine is divided into as many pieces as the number of axial ducts, and the symmetry is utilized. The geometry is discretized into 13 elements in the radial, 12 elements in the axial and 5 elements in the azimuthal direction.

The axial ducts are manufactured by using plastic rods during winding manufacturing and removing them after epoxy casting.

5) Annular Gap

Another method of bringing the coolant in the active region of the electrical machine is by introducing an annular gap between the winding and the air gap of the machine. Doing so, the coolant is also brought closer to

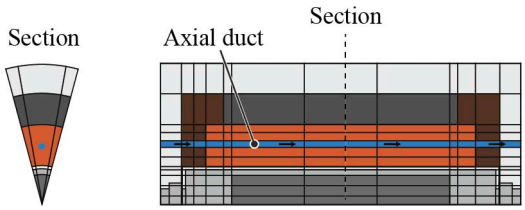

Fig. 8. Discretization of the machine geometry for the thermal analysis of the machine with axial ducts.

the rotor and therefore the heat is more easily removed from the rotor (via the air gap). The annular gap is separated from the air gap via a thin plastic wall such that water can be used without wetting the rotor and/or the bearings; and air can be used without an increase in the air-friction losses in the air gap. Similar to the axial ducts, the annular gap has to be dimensioned considering the trade-off between the thermal performance and the increase in copper losses. The annular gap considered in this work is 0.5 mm thick.

Fig. 9 shows the model describing the machine with an annular gap. The geometry is represented by 14 elements in the radial and 12 elements in the axial direction.

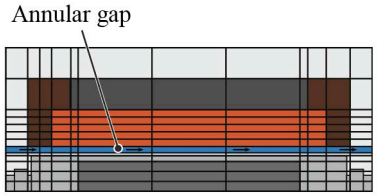

Fig. 9. Discretization of the machine geometry for the thermal analysis of the machine with an annular gap.

III. Experimental Verification

In order to verify the validity of the thermal modeling approach and to compare the four new cooling concepts to the state-of-the-art jacket cooling, five stators are manufactured, four of them equipped with the four new cooling concepts and one with the state-of-the-art jacket cooling. PT-100 temperature sensors are added in the winding as shown in Fig. 10, and digital multimeters are used to measure the temperatures. In order to simplify the manufacturing process, sensors are placed only at the center and one edge in the axial direction. However, the measurements can be repeated by reversed coolant flow direction in order to see the temperatures at coolant inlet and outlet sides of the machine. The sensors are azimuthally distributed in the winding pack in order not to modify the winding structure significantly. For stators employing graphite heat pipes and axial ducts, the azimuthal position is adjusted to measure the hot spot temperatures (e.g. sensor placed in the middle between two axial ducts).

As the main goal is the verification of the thermal models and comparison of the cooling methods, the following measurement approach is undertaken. A DC voltage is applied to the windings in order to generate

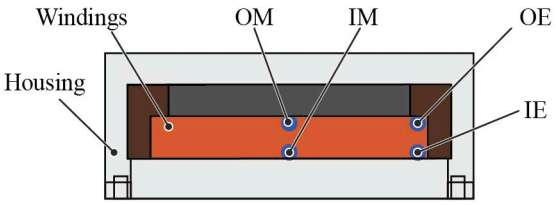

Fig. 10. Placement of the temperature sensors in the winding region for the experimental verification of the thermal models. The rotor and the bearings are not required and therefore not installed during measurements. The temperature sensors are named according to their location where 'O', 'I', 'E' and 'M' stand for outer, inner, end and middle, respectively.

copper losses. The required amount of losses is maintained by adjusting the voltage considering the temperature-dependent electrical resistances of the windings. This removes the uncertainty on the different loss components such as air friction and rotor losses and allows for a precise verification of the thermal models on the stator side. Rotors are not required for these tests, and therefore they are not installed. The air gap thermal conductivity is set to zero in the thermal models in order to mimic this measurement condition. Fig. 11 shows a photo of the stator with jacket cooling and the 3-D printed plastic structure that separates the annular gap from the air gap.

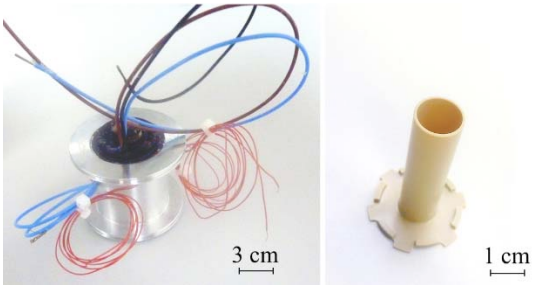

Fig. 11. (Left) Photo of the stator with jacket cooling. (Right) Plastic wall separating the annular gap and the air gap.

Fig. 12 shows simulated and measured winding temperatures for jacket cooling where the coolant is water and the flow rate is 16.6 g/s. Similarly, Fig. 13 shows simulated and measured winding temperatures for jacket cooling with air cooling and 1 bar relative pressure. It can be seen that the models and the measurements yield similar winding temperatures.

Fig. 14 compares simulation and measurement results for annular gap where water inlet temperature is 17°C and flow rate is 16.6 g/s. It can be seen that the models predict the location of the hot spots correctly, even though a certain mismatch exists between the modeled and measured temperatures. On the other hand, the rated copper losses of the machine are around 20 W, at which level the absolute temperature difference is within 1°C. The mismatch occurring at higher losses is the subject of ongoing research.

Fig. 15 shows the simulated and measured differences in winding temperatures when using an annular gap instead of jacket cooling at 60 W of copper losses. The water flow rate is 16.6 g/s, the coolant inlet temperature is 17°C. Similarly, Fig. 16 and Fig. 17 compare axial

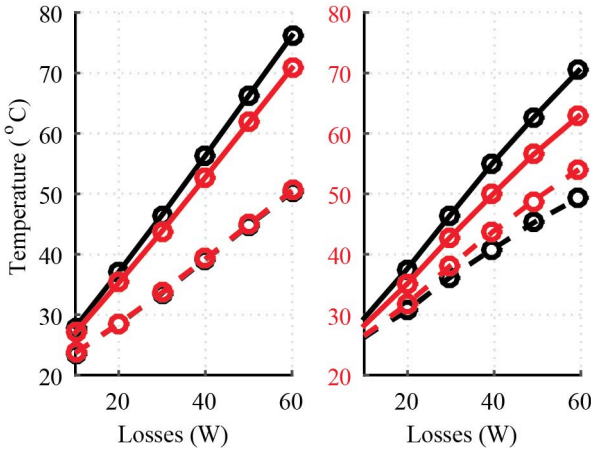

Fig. 12. (Left) Simulated and (Right) measured winding temperatures for jacket cooling and 16.6 g/s water mass flow. Solid lines denote inner and dashed lines denote outer sensors (radial direction). Black denotes middle and red denotes outlet side (axial direction).

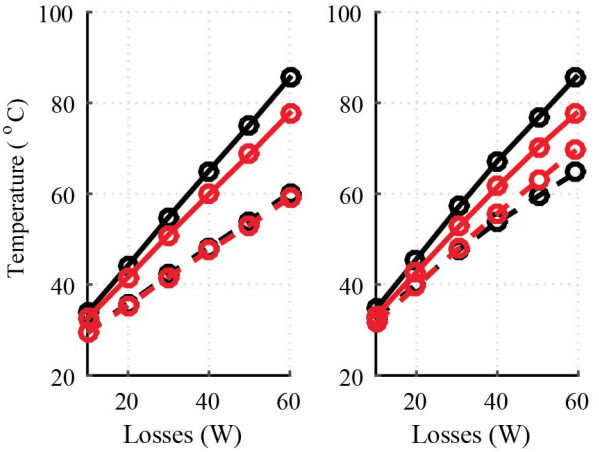

Fig. 13. (Left) Simulated and (Right) measured winding temperatures for jacket cooling and air cooling with 1 bar relative pressure. Solid lines denote inner and dashed lines denote outer sensors (radial direction). Black denotes middle and red denotes outlet side (axial direction).

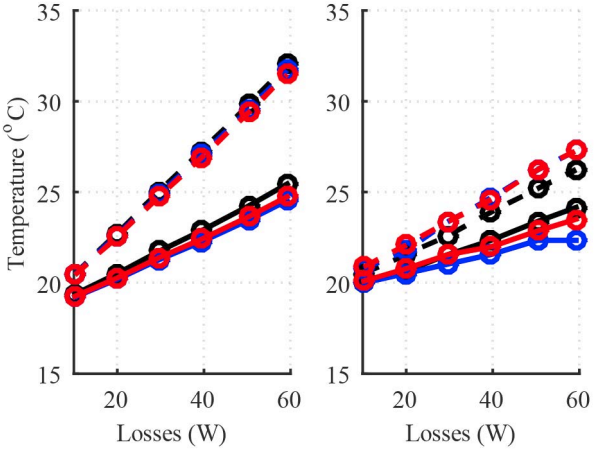

Fig. 14. (Left) Simulated and (Right) measured winding temperatures for the annular gap cooling with 17°C and 16.6 g/s water flow. Solid lines denote inner and dashed lines denote

ducts and toroidal windings to jacket cooling under similar conditions.

In general it can be concluded that the models predict the measurement results accurately. A winding hot-spot temperature decrease of more than 40°C is possible using the annular gap or axial duct concepts and water cooling. Toroidal windings also lead to lower winding temperatures; however, their increased copper resistances along with their higher winding factors need to be considered for a fair comparison.

A further advantage of the annular gap cooling against the other concepts described here is its ability to also cool the rotor better than the other methods, as the cooling channel is the closest to the air gap. This advantage becomes even more prominent when compared to different cooling approaches used in industry, e.g. an axial housing flange thermally coupled to the end windings.

Due to challenges in manufacturing, the graphite heat pipes have been covered by a polyimide tape and have been placed only at the inner and outer surfaces rather than inside of the winding pack, which has seriously hindered their cooling capability. Consequently, the implemented cooling system does not lead to any improvement compared to the jacket cooling. However, the graphite heat pipes remain an interesting option; as owing to their very thin geometries, the increase of losses due to the reduced winding area or due to the additional eddy-currents in the sheets remain very small. However, the thin geometry also makes it necessary to investigate alternative winding manufacturing methods where graphite sheets can be better integrated.

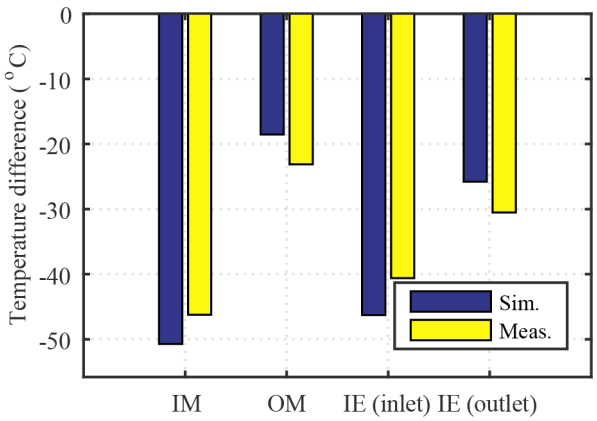

Fig. 15. Simulated and measured difference in winding temperatures when using an annular gap instead of jacket cooling. The water flow rate is 16.6 g/s for both cases and the losses are 60 W. Absolute temperatures of the sensor positions can be read from Fig. 12.

IV. Power Density Increase

In order to relate the winding temperature decrease enabled by a specific cooling method to the actual achievable power density increase, a coupled thermal and electromagnetic analysis of the machine is required. The reason behind this can be better understood considering the nonlinear increase in the rotor losses by the increased winding currents, or the nonlinear change of the thermal resistances into the coolants by changing temperatures. Moreover, the parameters defining the cooling concepts implemented in hardware (e.g. number of ducts, annular gap width etc.) in this paper are not resulting from a systematic optimization but rather from engineering intuition or limitations of the machine manufacturing process. However, as the validity of these computationally very efficient methods are demonstrated in this work, they can be easily integrated in the overall machine optimization procedure. Only after optimizing the thermal and magnetic designs of the machine together

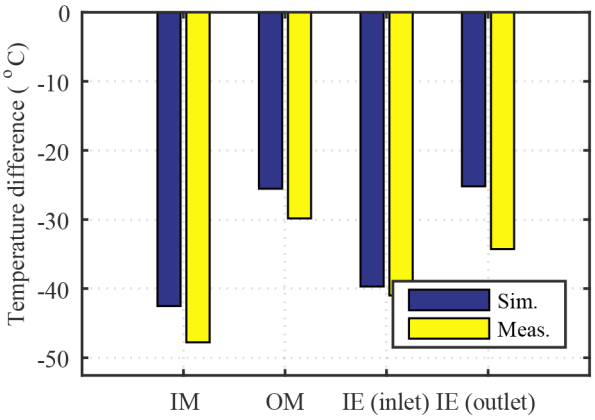

Fig. 16. Simulated and measured difference in winding temperatures when using axial ducts instead of jacket cooling. The water flow rate is 16.6 g/s for both cases and the losses are 60 W. Absolute temperatures of the sensor positions can be read from Fig. 12.

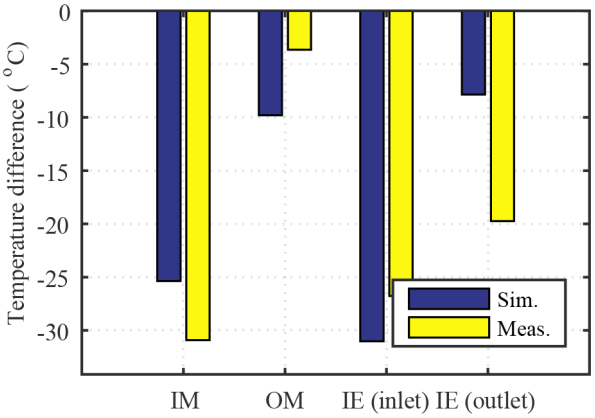

Fig. 17. (a) Simulated and measured difference in winding temperatures when using toroidal windings instead of jacket cooling. The water flow rate is 16.6 g/s for both cases and the losses are 60 W. Absolute temperatures of the sensor positions can be read from Fig. 12.

one can assess the achievable increase in power density. This is the scope of ongoing research.

Nevertheless, this section gives a simplified approach to determine the theoretical increase a specific cooling concept could lead to.

Even though pulse-amplitude-modulation (PAM) is currently more widely applied in high-speed drives [23], a major drawback of this modulation strategy is that the low frequency harmonic content of the phase current

increases significantly with increasing torque. This means a significant increase in rotor losses with increasing load. However, recent advancements in wide band gap power semiconductor technology (GaN, SiC) enables the use of pulse-width-modulation (PWM) instead of PAM. Using PWM, the dependency of the rotor losses on the torque is not as significant. Considering this, the increase of rotor losses by increasing torque is neglected here.

Comparing Fig. 12 and Fig. 14, the measured winding hot spot temperature rise can be read as 53°C for jacket cooling and 10°C for the annular gap cooling, at 60 W copper losses and 17°C coolant inlet temperature. Assuming a linear behavior, one can conclude in a first step that the windings reach the critical temperature of 120°C when the copper losses are 117 W for the jacket cooling and 618 W for the annular gap cooling. Neglecting the space required for the annular gap and assuming the same copper cross-sectional area for both machines, and assuming that the torque of the machine is proportional to the square root of the losses, the annular gap can be claimed to lead to a theoretical power density increase of up to $\sqrt{618/117} \approx 2.3$ times the jacket cooling. Considering a water flow rate of 16.6 g/s, the coolant temperature at the outlet in this case is 26°C.

V. Conclusions

This paper describes different forced cooling methods developed for slotless ultra-high-speed electrical machines. Lumped-parameter-based analytical models are developed to analyze the described methods. The presented methods are flexible, fast and sufficiently accurate; therefore, they can be incorporated into machine optimization.

The thermal models are experimentally verified using five stators, four of them employing the new cooling methods and one employing the state-of-the-art jacket cooling. More than 40°C winding temperature decrease is measured with two of the concepts (annular gap and axial ducts) compared to the state-of-the-art jacket cooling. Using a simplified scaling law, this is shown to lead to a theoretical increase of the power density by a factor of two in the best case. However, a complete machine optimization considering the thermal, magnetic and mechanical design of the machine needs to be carried out in order to show the actual achievable power density increase.

The future work will deal with the complete machine optimization described above. Furthermore, methods for measuring the rotor temperature during operation will be investigated.

References

[1] D. Gerada, A. Mebarki, N. Brown, C. Gerada, A. Cavagnino, and A. Boglietti, "High-speed electrical machines: Technologies, trends, and developments," *IEEE Trans. on Ind. Electr.*, vol. 61, no. 6, pp. 2946–2959, Jun. 2014.

[2] C. Zwyssig, S. Round, and J. W. Kolar, "An ultrahigh-speed, low power electrical drive system," *IEEE Trans. on Ind. Electr.*, vol. 55, no. 2, pp. 577–585, Feb. 2008.

[3] A. Borisavljevic, M. Kimman, P. Tsigkourakos, H. Polinder, H. Langen, R. Schmidt, and J. Ferreira, "Motor drive for a novel high-speed micro-milling spindle," in *IEEE/ASME Int. Conf. on Adv. Intel. Mech. (AIM)*, pp. 1492–1497, Jul. 2009.

[4] P.-D. Pfister and Y. Perriard, "Very-high-speed slotless permanent-magnet motors: Analytical modeling, optimization, design, and torque measurement methods," *IEEE Trans. on Ind. Electr.*, vol. 57, no. 1, pp. 296–303, Jan. 2010.

[5] D. Krahenbuhl, C. Zwyssig, H. Weser, and J. W. Kolar, "A miniature 500 000 r/min electrically driven turbocompressor," *IEEE Trans. on Ind. Appl.*, vol. 46, no. 6, pp. 2459–2466, 2010.

[6] S. Stevens, G. Deliege, J. Driesen, and R. Belmans, "A hybrid high speed electrical micromachine for micro scale power generation," in *IEEE International Conference on Electric Machines and Drives*, pp. 1135–1142, May 2005.

[7] C. Zwyssig, T. Baumgartner, and J. W. Kolar, "High-speed magnetically levitated reaction wheel demonstrator," *IEEE International Power Electronics Conference* (IPEC - ECCE Asia), pp. 1707–1714, May 2014.

[8] C. Zwyssig, S. Round, J. W. Kolar, "Megaspeed drive systems: Pushing beyond 1 million r/min," *IEEE/ASME Trans. on Mech.*, vol. 14, no. 5, pp. 564-574, Oct. 2009.

[9] D. Staton and A. Cavagnino, "Convection heat transfer and flow calculations suitable for electric machines thermal models," *IEEE Trans. on Ind. Electr.*, vol. 55, no. 10, pp. 3509-3516, Oct. 2008.

[10] D. Dorrell, "Combined thermal and electromagnetic analysis of permanent-magnet and induction machines to aid calculation," *IEEE Trans. on Ind. Electr.*, vol. 55, no. 10, pp. 3566-3574, Oct. 2008.

[11] P. Vong and D. Rodger, "Coupled electromagnetic-thermal modeling of electrical machines," *IEEE Trans. on Magn.*, vol. 39, no. 3, pp. 1614-1617, May 2003.

[12] Celeroton AG, "Datasheet CT-17-1000," Internet: www.celeroton.com, retrieved on: Apr. 2015.

[13] S. Ruoho and A. Arkkio, "Partial demagnetization of permanent magnets in electrical machines caused by an inclined field," *IEEE Trans. on Magn.*, vol. 44, no. 7, pp. 1773-1778, Jul. 2007.

[14] A. Boglietti, A. Cavagnino, D.Stator, M. Shanel, M. Mueller, and C. Mejuto, "Evolution and modern approaches for thermal analysis of electrical machines," *IEEE Trans. on Ind. Electr.*, vol. 56, no. 3, pp. 871-882, Mar. 2009.

[15] P. R. N. Childs and C. A. Long, "A review of forced convective heat transfer in stationary and rotating annuli," *Proc. of the Instit. of Mech. Eng. Sci.*, vol. 210, no. 123, pp. 123-134, Mar. 1996.

[16] Verein Deutscher Ingenieure, *VDI – Wärmeatlas*, Springer-Verlag Berlin Heidelberg, 3rd ed., 2009.

[17] J. Nerg, M. Rilla, and J. Pyrhönen, "Thermal analysis of radial-flux electrical machines with a high power density," *IEEE Trans. on Ind. Electr.*, vol. 55, no. 10, pages 3543-3554, Oct. 2008.

[18] J. Pyrhönen, T. Jokinen, and V. Hrabovcova, *Design of rotating electrical machines*, John Wiley and Sons, 1st ed., 2008.

[19] S. K. Mukerji, M. George, M. B. Ramamurthy, and K. Asaduzzaman, "Eddy currents in solid rectangular cores," *Prog. in Electromagn. Res. B*, vol. 7, pp. 117-131, 2008.

[20] D. Steinert, T. Nussbaumer, J. W. Kolar, "Slotless bearingless disk drive for high-speed and high-purity

applications," *IEEE Trans. on Ind. Electr.*, vol. 61, no. 11, pp. 5974-5986, Nov. 2014.
[21] E. Spooner, and B. J. Chalmers, "TORUS': A slotless, toroidal-stator, permanent-magnet generator," *IEE Proc. B Ele. Pow. Appl*., vol. 139, no. 6, pp. 497-506, Nov. 1992.
[22] C. Zwyssig, J. W. Kolar, W. Thaler and M. Vohrer, "Design of a 100 W, 500 000 rpm permanent-magnet generator for mesoscale gas turbines," *Conf. Rec. of the 40th IEEE Ind. Appl. Conf.*, (IAS), Oct. 2005.
[23] L. Schwager, A. Tüysüz, C. Zwyssig and J. W. Kolar, "Modeling and comparison of machine and converter losses for PWM and PAM in high-speed drives," *IEEE Trans. on Ind. Appl*., vol. 50, no. 2, pp. 995-1006, Mar./Apr. 2014.